

Diffuse optical spectroscopy measurements of healing in breast tissue after core biopsy: case study

Wendy Tanamai

Cynthia Chen

Sara Siavoshi

Albert Cerussi

University of California, Irvine
Beckman Laser Institute
Laser Medical and Microbeam Program
1002 Health Sciences Road East
Irvine, California 92612

David Hsiang

John Butler

University of California Irvine Medical Center
Department of Oncological Surgery
101 The City Drive
Orange, California 92868

Bruce Tromberg

University of California, Irvine
Beckman Laser Institute
Laser Medical and Microbeam Program
1002 Health Sciences Road East
Irvine, California 92612

Abstract. Diffuse optical spectroscopy (DOS) has been used to monitor and predict the effects of neoadjuvant (i.e., presurgical) chemotherapy in breast cancer patients in several pilot studies. Because patients with suspected breast cancers undergo biopsy prior to treatment, it is important to understand how biopsy trauma influences DOS measurements in the breast. The goal of this study was to measure the effects of a standard core breast biopsy on DOS measurements of tissue deoxyhemoglobin, hemoglobin, water, and bulk lipid concentrations. We serially monitored postbiopsy effects in the breast tissue in a single subject (31-year-old premenopausal female) with a $37 \times 18 \times 20$ mm fibroadenoma. A baseline measurement and eight weekly postbiopsy measurements were taken with a handheld DOS imaging instrument. Our instrument used frequency domain photon migration combined with broadband steady-state spectroscopy to characterize tissues via quantitative measurements of tissue absorption and reduced scattering coefficients from 650 to 1000 nm. The concentrations of significant near-infrared (NIR) absorbers were mapped within a 50 cm^2 area over the biopsied region. A 2-D image of a contrast function called the tissue optical index (TOI = deoxyhemoglobin \times water/bulk lipid) was generated and revealed that a minimum of 14 days postbiopsy was required to return TOI levels in the biopsied area to their prebiopsy levels. Changes in the TOI images of the fibroadenoma also reflected the progression of the patient's menstrual cycle. DOS could therefore be useful in evaluating both wound-healing response and the effects of hormone and hormonal therapies *in vivo*. © 2009 Society of Photo-Optical Instrumentation Engineers. [DOI: 10.1117/1.3028012]

Keywords: near-infrared (NIR); photon migration; tissue spectroscopy; frequency-domain photon migration; breast cancer; hormonal response; menstrual cycle.

Paper 07345RR received Aug. 23, 2007; revised manuscript received Sep. 3, 2008; accepted for publication Sep. 3, 2008; published online Jan. 20, 2009.

1 Introduction

1.1 Optical Monitoring of the Effects of Neoadjuvant Chemotherapy

Neoadjuvant chemotherapy, or chemotherapy administered prior to the surgical removal of the tumor, is increasingly used for treatment of large (>2 cm) and locally advanced breast cancers.¹⁻³ Neoadjuvant chemotherapy offers two distinct advantages over conventional postsurgical chemotherapy. First, neoadjuvant chemotherapy reduces tumor size prior to surgery, thereby increasing the potential for breast-conserving procedures. Second, neoadjuvant chemotherapy provides physicians an opportunity to evaluate the effectiveness of the treatment on the patient's tumor. Because therapeutic effectiveness can be quantified, alternative treatment regimens may be implemented if the initial treatment is ineffective. The *in vivo* evaluation of tumor response to therapy is of particular importance as new treatment options, particularly targeted

therapies, become increasingly available for treating breast cancer.

Diffuse optical spectroscopy (DOS) and diffuse optical imaging (DOI) have been suggested as techniques that could monitor the physiological effects of neoadjuvant chemotherapy.⁴⁻⁸ DOS is a noninvasive, bedside-capable technique that quantitatively measures near-infrared (NIR, 650 to 1000 nm) absorption and reduced scattering spectra.⁹ Absorption spectra are used to calculate the tissue concentrations of oxygenated (ctO₂Hb) and deoxygenated hemoglobin (ctHHb), water (ctH₂O), and bulk lipid, which are the dominant NIR molecular absorbers in breast tissues. DOS does not require exogenous contrast and rapidly (<10 s) provides quantitative, functional information about tumor biochemical composition, making it potentially desirable from a patient perspective. Typically, DOS samples a low number of spatial locations with a large spectral bandwidth. In contrast, DOI typically samples a large number of spatial locations but with low spectral bandwidth. The relationship between DOS and

Address all correspondence to Albert Cerussi, University of California, Irvine, Beckman Laser Institute, Irvine, California 92612. E-mail: acerussi@uci.edu

DOI is comparable to that between magnetic resonance spectroscopy (MRS) and magnetic resonance imaging (MRI).

In early-stage clinical studies, DOI and DOS have been used to characterize breast tumor biochemical composition and monitor therapeutic response in Stage II/III patients undergoing neoadjuvant chemotherapy. We have reported the use of DOS to track long-term tumor response to neoadjuvant chemotherapy in a human subject.⁵ Changes in tissue biochemical composition were quantified over a three-cycle, 68-day Adriamycin/Cytosin (A/C) regimen. Significant reductions in total tumor hemoglobin concentration (ctTHb) and ctH₂O of 56% and 67%, respectively, were observed by the final treatment. Recent studies have supported these findings by comparing optical imaging with MRI and ultrasound after long-term treatment.⁶⁻⁸

More recently, DOS measurements obtained prior to and 1 week into treatment were used to predict final, postsurgical pathological response, as demonstrated in an 11-patient pilot study.⁴ Tumor concentrations of ctHHb, ctO₂Hb, and ctH₂O dropped $27 \pm 15\%$, $33 \pm 7\%$, and $11 \pm 15\%$, respectively, within 1 week (6.5 ± 1.4 days) of the first treatment for pathology-confirmed responders ($N=6$), while nonresponders ($N=5$) and contralateral normal controls showed no significant differences in these parameters. Tumors displaying higher pretreatment levels of tumor ctO₂Hb relative to normal tissues also were more likely to respond to neoadjuvant chemotherapy. These results highlight DOS sensitivity to tumor cellular metabolism and biochemical composition and demonstrate its potential for predicting and monitoring an individual's response to treatment.

1.2 Challenges Presented by Clinical Biopsies

Because our goal is to introduce DOS as a monitoring tool for neoadjuvant chemotherapy in breast cancer, we must investigate how optical measurements may be influenced by clinical standard-of-care. Biopsy is routinely performed on any suspicious lesion found in the breast via clinical exam or screening mammography. Neoadjuvant chemotherapy may then be prescribed if malignancy has been documented on pathologic review. In general, neoadjuvant chemotherapy is started within days to weeks following pathological confirmation, depending on a variety of factors.¹⁰ The inflammatory response and post-procedural bleeding introduced by biopsy, however, present challenges for noninvasive imaging in general, and optical imaging in particular.

1.3 Effects of Wound Healing

A biopsy is a tissue-injuring wound that causes the disruption of blood vessels, leakage of blood constituents, inflammation, and bruising.¹¹ The wound-healing response undergoes several overlapping phases: hemostasis, inflammation, proliferation, and remodeling. Hemostasis occurs over minutes after the biopsy. During the inflammatory phase (generally three days post injury), vasodilation occurs, which increases blood flow into the surrounding tissues. In addition, macrophages begin to secrete growth factors such as fibroblast growth factor (FGF-1, FGF-2) and vascular endothelial growth factor (VEGF). These growth factors eventually lead to angiogenesis and resultant blood vessel migration into the wound.¹²

The proliferative phase, occurring 3 to 12 days after, mainly involves the production of granulation tissue. Granulation tissue also consists of macrophages, fibroblasts, and blood vessels. The macrophages provide a continuing source of growth factors needed to stimulate fibroplasia and angiogenesis. Remodeling, the longest phase of soft-tissue wound healing, takes several months to complete. Collagen remodeling takes place as granulation tissue is replaced with type I collagen, elastin fibers, proteoglycans, and glycoproteins. As wounds mature and fill with granulation tissue, angiogenesis ceases, and fibroblasts and inflammatory cells slowly disappear as a result of apoptosis.^{11,13} In addition, the wound is remodeled and blood flow decreases as a result of fewer blood vessels.

Several studies have been conducted to monitor cutaneous wound healing through such techniques as photography,¹⁴ odor,¹⁵ and sonographic monitoring.¹⁶ Yet, fewer studies have been conducted on monitoring soft tissue wound healing, particularly using quantitative methods.

1.4 Project Goals

Our study was designed to determine the amount of time required for the breast to heal from a standard-of-care core biopsy such that DOS/ DOI measurements would be unaffected. Prior to biopsy, a lesion was imaged using a handheld DOS instrument. After the biopsy, the lesion was manually scanned weekly for 8 weeks to quantify the impact of the biopsy within the field of view of the DOS instrument. Based on the current literature stating that the major phases of wound healing would be complete after 4 weeks, we decided to continue evaluating the patient beyond that time frame to ensure that all healing effects could be observed. By quantifying the time scale for wound healing, the time frame needed to minimize biopsy effects on DOS measurements could then be determined.

2 Methods

2.1 Laser Breast Scanner Instrument

Specific details of our DOS instrument, the laser breast scanner (LBS), have been previously described in detail.⁹ Briefly, the current LBS instrument is a bedside-capable, multiwavelength device that integrates both broadband frequency-domain and broadband steady-state approaches to provide complete tissue absorption and scattering spectra from 650 to 996 nm. Briefly, the frequency-domain component employs six fiber-coupled diode lasers (658, 682, 785, 810, 830, and 850 nm) and an avalanche photodiode (APD) detector. Each laser diode is swept in modulation frequency from 50 to 500 MHz in 401 steps.¹⁷ The steady-state component employs a fiber-coupled broadband lamp and a fiber-coupled back-illuminated CCD spectrometer (BW Tek, Newark, Delaware). A handheld probe was designed such that both frequency-domain and steady-state approaches interrogated the same region of breast tissue. The source-detector separation distance was fixed at 28.5 mm in a reflection-style geometry. Measurement time was less than 10 s per spatial location for both frequency-domain and steady-state measurements combined. Calibrations for the frequency-domain and steady-state instruments were performed using a tissue phantom and an integrating sphere, respectively.

Simple calculations using known absorber extinction coefficients were used to convert the recovered absorption spectra into the tissue concentrations of deoxyhemoglobin (ctHHb, in μM), oxyhemoglobin (ctO₂Hb, in μM), water (ctH₂O, in %), and bulk lipids (Lipid, in %), which are the primary NIR absorbers in breast tissue.^{18–20} ctH₂O is the concentration of measured tissue water divided by pure water concentration (55.6 M), whereas tissue lipids are reported as the percentage lipid measured relative to an assumed “pure” lipid density of 0.9 g mL⁻¹. Thus, reported water and lipid percentages are relative figures of merit compared to pure solutions of the substance and are neither strict volumes nor add to 100%. The reduced scattering properties of tissue are reported as the results of a power-law fit to the measured frequency-domain reduced scattering values.²¹ The absolute value of the exponent resulting from this fit is termed the scatter power (SP), and the prefix is termed the scatter amplitude (A). In general, the SP is related to the size of the tissue scattering particles in relation to the optical wavelength, and the A is related to the density of the scattering centers. A tissue optical index (TOI) was also calculated according to the formula $\text{TOI} = \text{ctHHb} \times \text{ctH}_2\text{O} / \text{Lipid}$. The TOI has been shown to be a useful index for the detection of malignant breast lesions by combining the highest-contrast parameters into a single expression.⁹ All calculations were performed using custom algorithms developed within the MATLAB platform.

2.2 Measurement Sequence

A single subject was recruited for this case study. The subject provided informed written consent to participate in this research study, which was approved by the University of California, Irvine, Institutional Review Board (Protocol #95-563). The subject was a 31-year-old female with a suspicious mass in the right breast at the 3 o'clock position 1 to 3 cm from the nipple. Standard clinical ultrasound indicated that the lesion was well circumscribed and homogeneous, measuring 3.7 by 1.8 by 2.0 cm.

LBS measurements were performed on the subject over an 8-week cycle (Table 1). The initial LBS measurement was taken 4 days prior to a standard core biopsy. Pathology indicated that the sampled lesion was a benign fibroadenoma. Subsequent LBS measurements were performed weekly thereafter to monitor breast optical properties throughout the wound-healing process, as outlined in Table 1; a total of eight postbiopsy LBS measurements were performed. Because the subject was premenopausal, we also related LBS measurement dates to patient menstrual cycle phases. In order to approximate the subject's phase in menstrual cycle, menses onset dates were recorded. The menstrual cycle length was calculated as the first day of the menses to the last day before next menses. The assumption that the luteal phase is approximately 14 days prior to the onset of menses was used to postulate when the ovulatory phase occurred.

2.3 Diffuse Optical Spectroscopy Measurement Technique

Care was taken to perform LBS measurements with the patient in a consistent position. The subject laid supine with her arm up above her head on a recliner at about 30 deg from horizontal for all LBS measurements. An ultrasound was then

Table 1 Laser breast scanner measurement schedule.

Date	Measurement day relative to biopsy ^a	Day in menstrual cycle ^a	Approximate phase in cycle
7/21/2006	-4	-14	Luteinizing hormone surge
7/25/2006	0	-9	
8/3/2006	9	1	Menses
8/11/2006	17	8	
8/17/2006	23	14	
8/24/2006	30	21	Luteinizing hormone surge
8/31/2006	37	28	
9/7/2006	44	35	Volume high
9/14/2006	51	5	Menses
9/21/2006	58	12	

^aNegative values indicate days prior to known menstrual start date.

performed to visualize the breast lesion position at the time of the baseline LBS measurement. A steady-state broadband-only scan was done to quickly visualize the areas of greatest optical attenuation over the lesion localized by ultrasound. The point of highest attenuation was assumed to be the best representation of the lesion and was chosen as the center of the LBS scan area (Fig. 1(a)). A 10-mm-spaced point grid measuring 50 by 100 mm was marked on the breast using a nonpermanent surgical skin marker. Within our coordinate system, the nipple was taken to be the origin, with the LBS scan area centered on the (30 mm, 0 mm) location. The large scan area was chosen to cover regions of the breast both with

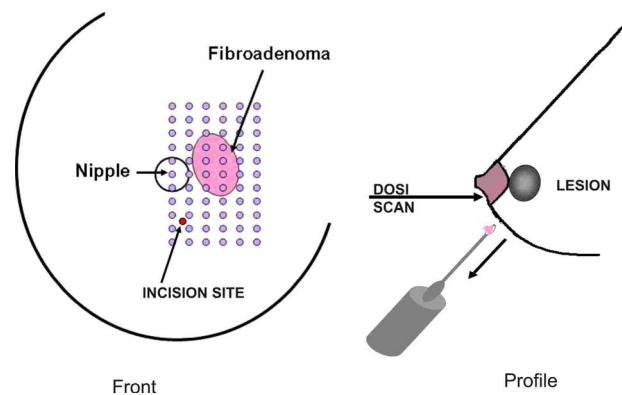


Fig. 1 (Left) Areas of the breast mapped by the LBS. Each small circle represents a single LBS measurement. Complete absorption and reduced scattering spectra were obtained at each spatial location. Measurements were also conducted on the contralateral normal side for comparison. (Right) Trajectory of the biopsy needle in a medial-lateral view. Notice that the needle direction lies under the LBS measurement area. Thus, the direction of the biopsy was not orthogonal to the mapped breast surface.

and without the lesion. The top leftmost point of the grid (0 mm, 50 mm) was measured with respect to the nipple and recorded to remark the LBS scan area on the subject during subsequent LBS measurements. On the contralateral normal breast, a partial grid covering the same area as the lesion was also marked and measured as a control. LBS measurements were performed at each spatial grid location by moving the handheld probe to each marked location. The instrument probe was placed with light gravitational pressure without compression on the skin surface. The average penetration depth of the light was calculated to be approximately 15 mm below the surface of the skin.

Maps of breast tissue physiological properties were generated by calculating the DOS-measured parameters at each grid location.⁹ No tomographic reconstructions were used, and the tissue within the field of view was assumed to be homogeneous in accordance with the standard diffusion approximation. Map points were interpolated using 2-D nearest-neighbor cubic splines to round out the discrete shapes. All image thresholds were performed using the maximum and minimum values of the image. A four-stage color bar was used with RGB values of (0,0,0), (0,0,255), (0,255,255), and (255,255,255) to display all functional maps.

The lesion center was defined as the spatial location of the TOI maximum in accordance with our previous studies.⁹ The spatial extent of the lesion was then defined as the full width at half maximum (FWHM) of the TOI image, as we have done for a single axis in previous nonimaging studies. The TOI FWHM image then formed a mask for the images of other optical properties. Because of the limited spatial sampling of the lesion (i.e., only a few points are typically found inside the uninterpolated lesion masks), we have reported the maximum value within the FWHM as a value representative of the lesion Feature-based stratification was preferred to a strict spatial segmentation of lesion area to guard against possible movement of the lesion and/or optically scanned area. Normal tissue values were taken to be the average of DOS-measured parameters from the same spatial location on the contralateral normal breast. The calculated standard deviations, typically from the background and other normal tissue regions, represents the variation in the measured parameter across the image area. Images were rethresholded by TOI FWHM for each measurement date.

2.4 Ultrasound

An ultrasound of the lesion was performed in order to determine the position, orientation depth, and size (Fig. 2). Ultrasound showed a well-circumscribed, solid mass at the 3 o'clock position of the right breast, 1 to 3 cm from the nipple. The ultrasound was taken in two views: transverse and longitudinal. The lesion dimensions in the transverse and longitudinal orientations were measured to be approximately 26.8×21.3 mm and 20.6×20.8 mm, respectively.

2.5 Needle Core Biopsy

A needle core biopsy was administered by a general surgeon 4 days after a baseline DOS measurement session. An incision was made at the surface of the breast at a site away from the lesion [Fig. 1(a)]. Figure 1(b) depicts the orientation of the biopsy needle in relationship to the lesion location and the

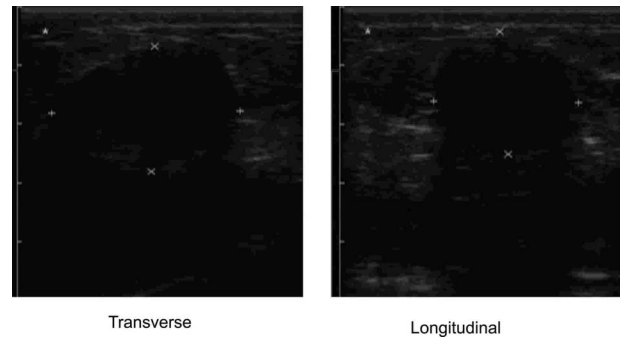


Fig. 2 Ultrasound profiles of the fibroadenoma in transverse (left) and longitudinal (right) profiles.

DOS scan in a medial-lateral view. The needle was inserted through the incision site and tracked through the lesion in the breast (dotted line). The LBS scan area was performed in the direction indicated in the figure. The position of the incision site was noted at each DOS measurement. On day 9, the incision scar was red and about the same size as the tip of the surgical marker used to mark the breast. The patient claimed the area was tender, but there was no irritation or bruising visible. By day 23, the redness at the site of incision had completely dissipated. On day 44, the patient reported that her breasts felt swollen. Her menses began on day 46.

3 Results

3.1 Fibroadenoma Functional Properties

Figure 3 displays a 5×10 cm spatial map of (a) ctHHb and (b) ctH₂O of the lesion and surrounding normal tissue 4 days prior to biopsy. The lesion area is the optical property in question that is above a threshold of the TOI FWHM. In agreement with our past broadband spectroscopic studies of benign²² and malignant⁹ lesions, Fig. 3 displays elevated water and hemoglobin concentrations relative to normal background tissue. The dark region on the left of the map is the areola, which was manually filtered from the map. ctH₂O and ctHHb are on average 19 and 33% respectively higher in the lesion compared to normal tissue. If we constrain the lesion to the signal above the parameter FWHM, the lesion size is approximately 20 by 30 mm. However, we note that the peak values of ctH₂O and ctHHb are not always colocalized.⁹

The baseline lesion map of the TOI contrast function is presented in Fig. 4. The TOI map displays features similar to both ctH₂O and ctHHb maps. The FWHM of the baseline TOI map is provided in Fig. 4(b); TOI values within the FWHM were averaged together to provide a value representative of the lesion. All DOS-measured parameters (i.e., ctHHb) were averaged over the same TOI FWHM thresholded area.

3.2 Serial Tissue Optical Index Maps

Figure 5 presents a series of lesion TOI maps taken over the course of an additional 8 weeks in the same human subject. Note that all maps have been rescaled to the maximum and minimum TOI values for comparison (which is mostly dominated by day 9). The initial map was acquired at baseline (4 days prebiopsy), with subsequent maps measured on dates

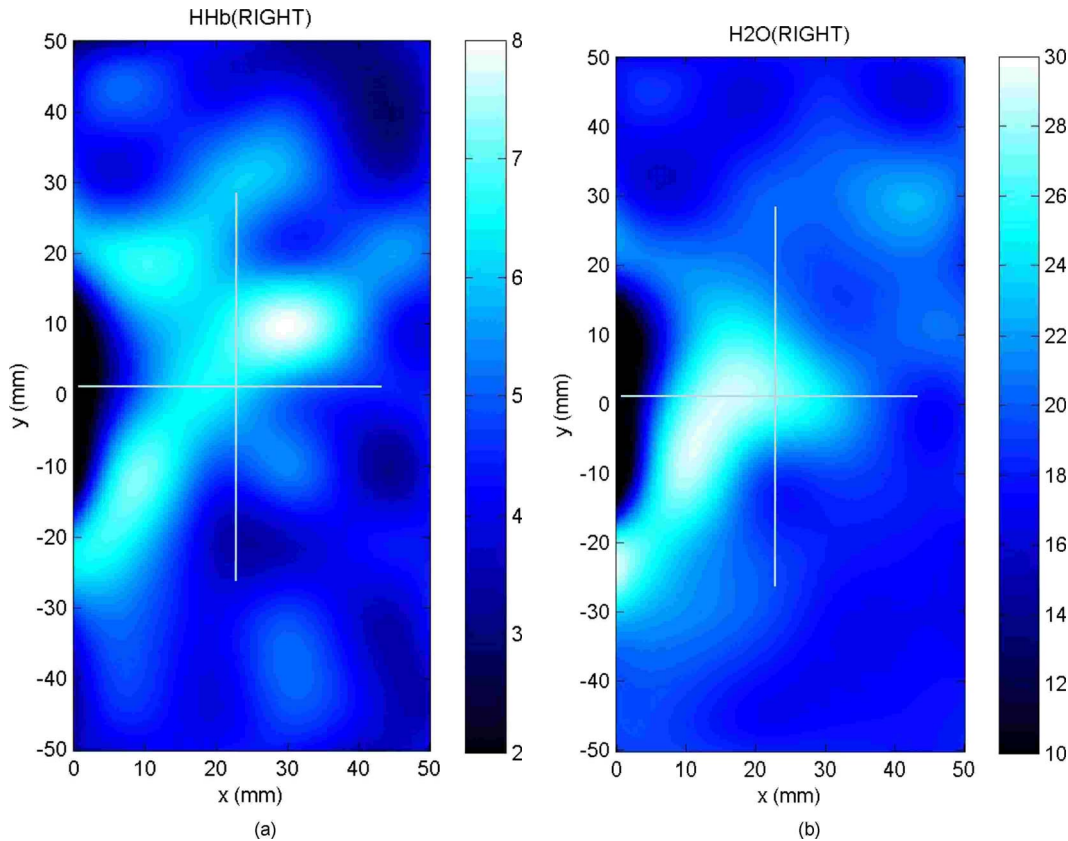


Fig. 3 Maps of the fibroadenoma optical properties prior to biopsy: (a) deoxyhemoglobin concentration and (b) water concentration. The areola region on the far-left side of the map was filtered out of each image.

listed in Table 1. The TOI map measured 9 days postbiopsy demonstrated a clear localized (10×10 mm) TOI increase in the vicinity of the lesion, which was likely the result of the biopsy via inflammation and bleeding. A general decreasing trend in TOI followed, which returned to baseline values 23 days postbiopsy. Several weeks after the initial biopsy, however, the TOI continued to oscillate, demonstrating another return to TOI baseline 51 days postbiopsy. We note that the “tail” region in the lower-left corner of the baseline image was still present in subsequent images when independently scaled, but it is not visible in this figure upon matching scales.

3.3 Image Analysis

Figure 6(a) provides a quantitative analysis of the previous lesion maps to facilitate comparisons; Figure 6(b) does the same for normal regions of the breast. “Lesion” values represent the peak TOI value within the TOI FWHM; in general, only a few actual DOS measurements were found within the TOI FWHM. “Background” values represent the average of the points in the same map that were below the TOI FWHM threshold, covering approximately a 40×80 mm field of view. “Normal” values were averaged over all map points taken from the contralateral breast. No distinction is made between lesion and biopsy areas because our low spatial sampling makes it hard to reliably separate the two areas.

The maximum TOI values show a clear peak at day 9, followed by an oscillatory behavior, in accordance with the images from Fig. 5. Although it is difficult to test for statisti-

cal significance with large disparity between sampled points (many in background, few in lesion), we can test to see that the background and lesion values are correlated. The background and lesion TOI values are strongly correlated, both with ($R^2=0.72$, $p=0.0039$) and without ($R^2=0.67$, $p=0.013$) the inclusion of day 9. More importantly, the weekly changes in background and lesion TOI are also correlated, both with ($R^2=0.61$, $p=0.022$) and without ($R^2=0.58$, $p=0.062$) the inclusion of day 9. These correlations suggest that the TOI changes in both background and lesion tend to track each other. In terms of TOI values averaged over the lesion FWHM at baseline, the average lesion TOI value was 2.20 ± 0.54 , with an average background TOI value of 1.20 ± 0.21 and an average normal TOI value of 1.12 ± 0.17 . The maximum averaged TOI value was 3.03. The average lesion TOI also followed an oscillatory pattern, with a period of approximately 4.5 weeks. The higher peak (day 9) is the result of the biopsy, as described earlier.

Figure 7 presents a quantitative analysis of the lesion maps for all other DOS-measured basis parameters in order to understand the origin of TOI changes in Fig. 6. In each panel, we plot the lesion maximum value (top plot), along with the average value and standard deviation of the normal tissue value (bottom plot). Panel (a) is the tissue water: there is a large increase on day 9 from the biopsy, and also a mild increase in a nearly periodic trend nearly 4 weeks later. The ctHHb does not display this behavior [panel (b)] with a rather flat distribution in the normal tissue. The lesion increase oc-

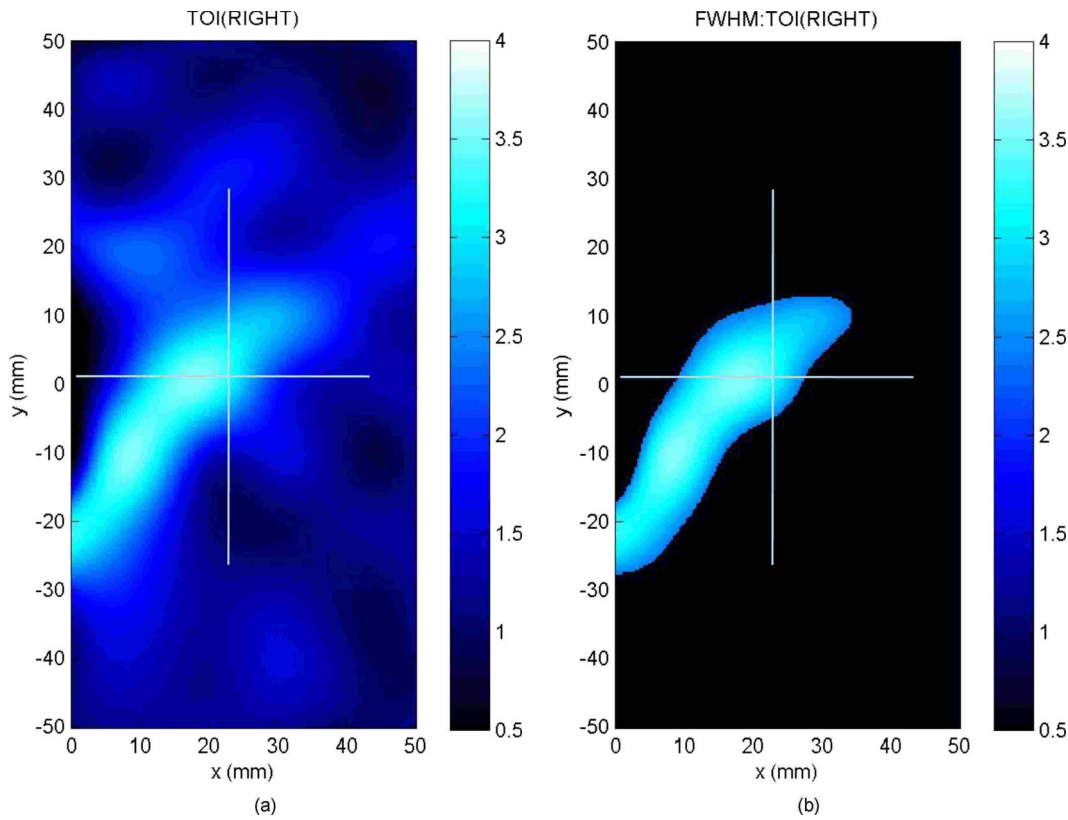


Fig. 4 Baseline maps of fibroadenoma TOI. (a) Standard TOI map, using data from the previous figure. (b) Full width at half maximum (FWHM) of the baseline TOI image. The TOI values within the FWHM were averaged to provide a tumor-averaged TOI value. For other parameters, the same area was used for the average; thus, for ctHHb, the same area as the FWHM of the TOI was used for the tumor-averaged ctHHb value.

curs after day 9. ctO₂Hb and lipids do not show remarkable features [panels (c) and (d), respectively], although the lipids do decrease in the latter portion of the measurements. The log of the scatter amplitude [LN(A)] in panel (e) shows a significant increase on the day of the biopsy and also later in the cycle on day 44; this second increase does not seem to coincide with the observed TOI changes. Tumor and normal are plotted on different scales to emphasize the relative magnitude of the changes in each tissue. Thus, it appears that the water increase and slight lipid decrease are most responsible for the increased TOI.

4 Discussion

4.1 Wound-Healing Response

The changes observed in DOS-measured parameters following breast biopsy were consistent with known soft tissue healing responses. Day 9 postbiopsy corresponds to the proliferation and remodeling phases of healing where blood flow increases and fluids accumulate in the injured tissue.²³ Alterations to the extracellular matrix also occur through the formation of granulation tissue and collagen.²⁴ The 10% increase in DOS-measured ctHHb, 65% increase in ctH₂O, and 43%

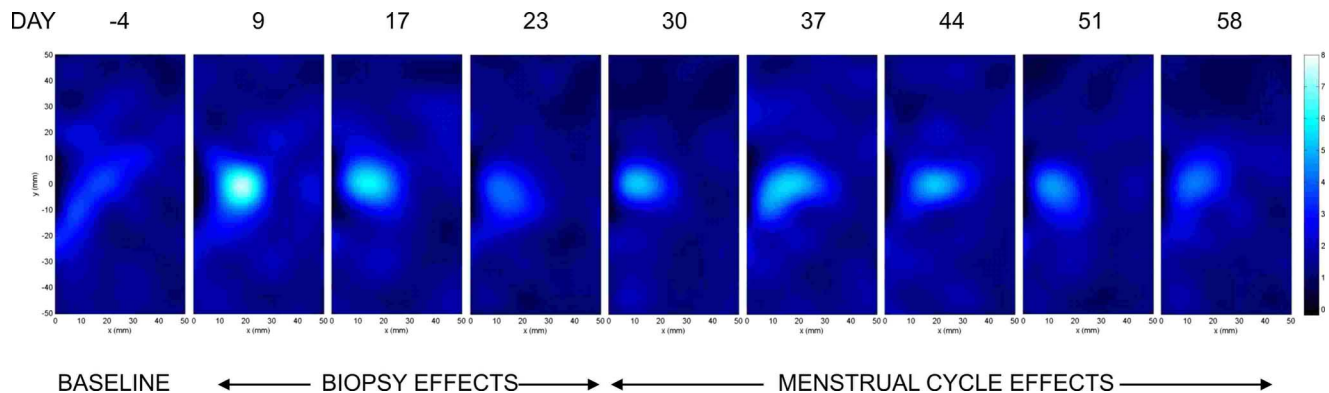


Fig. 5 Long-term changes in lesion TOI. Each map was scaled to the same maximum and minimum for comparison.

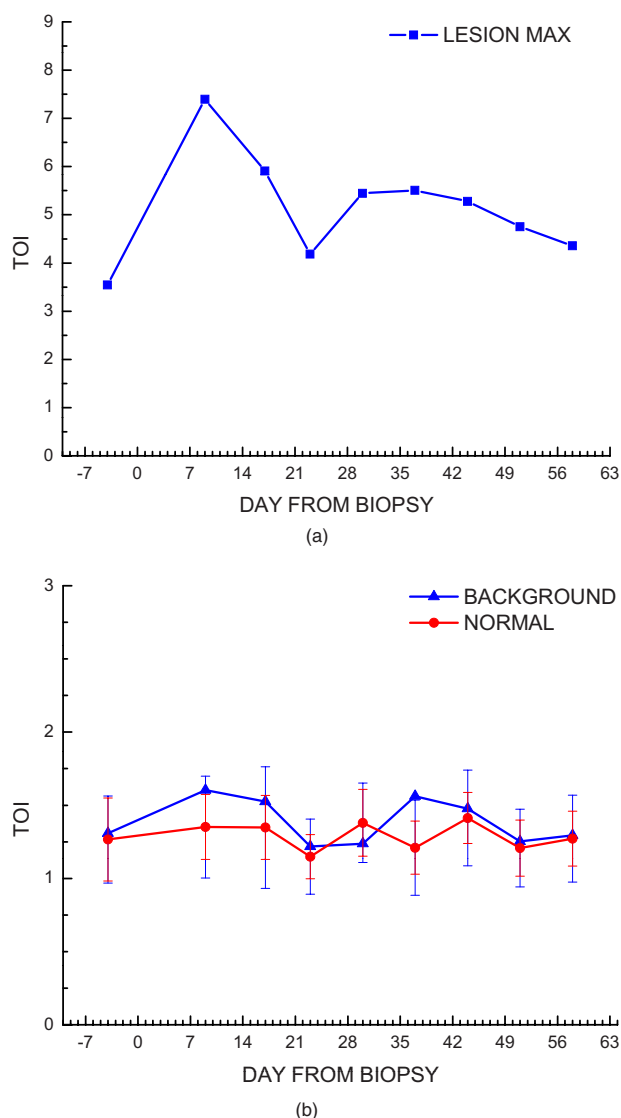


Fig. 6 Summary of serial TOI map analysis for the lesion. (a) The average values for each DOS-measured parameter averaged over the lesion TOI is provided. The error bars represent the degree of variance over the averaged area, and thus represent the heterogeneity of the tissue. (b) TOI for the remaining tissue in the lesion-containing breast and contralateral normal breast.

increase in LN(A) at day 9 are most likely due to these effects. These results are all significant when compared to the normal fluctuations seen in the normal breast on the same day, where ctHHb increased 13%, ctH₂O increased 8%, and LN(A) increased by 9%.

ctHHb, ctH₂O, LN(A), and TOI values recovered to their baseline values by day 23 postbiopsy. On day 23, we also noted that the surface on the incision scar visually healed. Therefore, in this patient, we assumed that the effects of the biopsy on DOS optical parameters dissipated after approximately 3 weeks. Individual response rates may vary with different patients, but the 2- to 3-week wound healing time frame is consistent with what has been reported by Hom.²³ The presence of bruises may prolong these effects, and thus

our case study may not represent the full spectrum of possible healing responses.

Past studies reporting the effects of chemotherapy upon tissue optical properties have shown a 26% and 37% decrease in hemoglobin and water, respectively, within the first 5 days of therapy.⁹ By comparing this to the 10% and 65% increase observed in hemoglobin and water 9 days postbiopsy, it is evident that the effects of biopsy must be accounted for or avoided before monitoring lesion changes. The effects of the wound-healing process must be deconvolved from any lesion shrinkage or growth effects.

4.2 Menstrual Cycle Fluctuations

Close inspection of the data on both biopsied and normal breasts revealed that functional changes continued well after the effects of the biopsy should have dissipated. Furthermore, the period of these changes roughly approximated the length of the menstrual cycle. Although only a few optical studies of breast physiology in the menstrual cycle have been conducted, these studies have demonstrated that measurable functional changes exist in some patients.²⁵⁻²⁷ Mammographic density fluctuations resulting from the menstrual cycle appear to depend upon overall breast density, so that we expect considerable variation in these functional changes across patients.²⁸

Studies have shown increases in breast tissue vascularity and density during the midluteal phase, as well as increases in breast volume during the end-luteal phase of the menstrual cycle.²⁵⁻²⁸ These processes were observed in the biopsied breast through increases in hemoglobin, scatter power, and water, during the midluteal phase (postbiopsy day 37), as well as through an increase in water during the end luteal phase (postbiopsy day 44). Although the normal breast followed these trends in ctO₂Hb, ctH₂O, and bulk lipid, it did not follow in ctHHb or LN(A).

The greater variation in DOS parameters in the biopsied breast suggests that the lesion was more sensitive to hormonal fluctuations brought on by the menstrual cycle than the normal breast tissue. This observation has important implications. Clearly, the timing of the menstrual cycle should be taken into account for diagnostic imaging, as is done for other imaging modalities. The same effect can have significant implications for longitudinal studies. For example, TOI decreases may not be due to reductions in angiogenesis, but instead due to menstrual-induced hormonal fluctuations. Alterations in lesion functional properties in response to hormonal variations may have further implications. The use of hormonal therapies (i.e., estrogen receptor targets, aromatase inhibitors) may necessitate a direct evaluation of lesion hormonal response. Biochemical changes in a lesion have been shown to be important for evaluating response to neoadjuvant chemotherapy,⁴ but hormonal response from endogenous and exogenous hormones, be they estrogen agonists or antagonists, may be equally important for making proper therapeutic choices. Further study will be required.

5 Conclusions

Our study illustrates that alterations of breast tissue biochemistry resulting from a biopsy and endogenous hormonal stimulation may be quantified using DOS. The effects of the biopsy

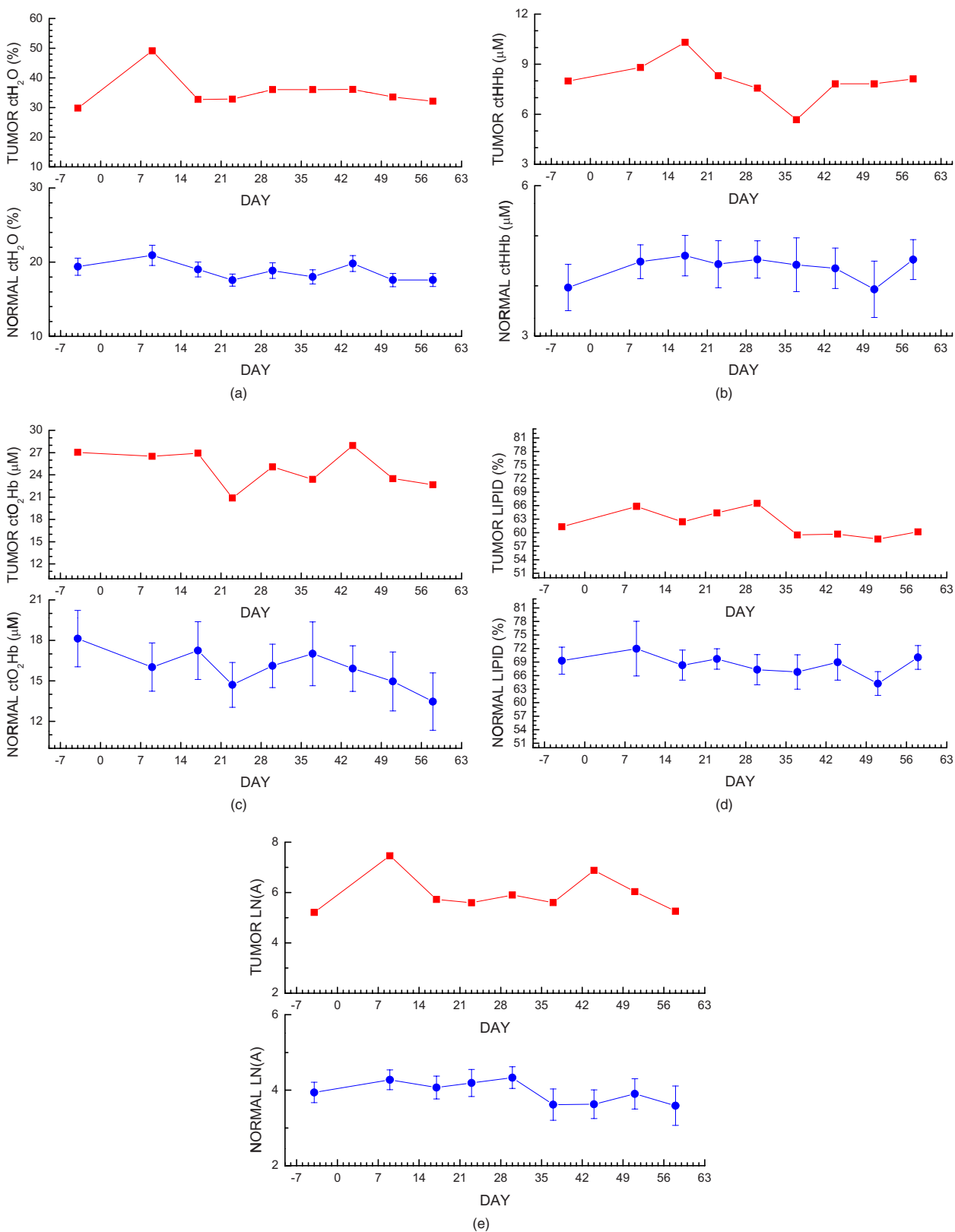


Fig. 7 Summary of serial map analysis for the lesion, but for all DOS-basis parameters. For the tumor tissue (top panels), the max value is plotted (as in Fig. 6). For the normal tissue (bottom panels), the average value, with standard deviation, is plotted. For normal tissues, the variations are about 4% (ctH₂O), 3% (lipids), 14% (ctO₂Hb), 10% (ctHHb), and 10% (LN(A)).

in this patient subsided after approximately 3 weeks, which is generally expected during the wound-healing process. While patient healing response will vary, we expect that 3 weeks should be sufficient for the effects of a biopsy to not interfere with DOS and DOI. We note that for large lesions, which are typical in neoadjuvant chemotherapy, it may be possible to biopsy one region of the lesion and optically sample the remainder of the lesion. We further demonstrated that the menstrual cycle affects both normal and lesion optical properties. The hormonal sensitivity of a lesion may impact future studies of breast cancer therapeutic response to hormonal agents.

Acknowledgments

This work was supported by the National Institutes of Health under grants Grant Nos. P41-RR01192 [Laser Microbeam and Medical Program (LAMMP)] and U54-CA105480 [Network for Translational Research in Optical Imaging (NTRIO)], the California Breast Cancer Research Program, and the Chao Family Comprehensive Cancer Center (P30-CA62203). Beckman Laser Institute Programmatic support from the Beckman Foundation and the Medical Free Electron Laser Program (AFOSR) is gratefully acknowledged. The authors wish to thank Montana Compton for her assistance with organizing the clinical trial and the patient who cheerfully volunteered her time to participate in this study.

References

1. I. C. Smith, S. D. Heys, A. W. Hutcheon, I. D. Miller, S. Payne, F. J. Gilbert, A. K. Ah-See, O. Eremin, L. G. Walker, T. K. Sarkar, S. P. Eggleton, and K. N. Ogston, "Neoadjuvant chemotherapy in breast cancer: significantly enhanced response with docetaxel," *J. Clin. Oncol.* **20**(6), 1456–1466 (2002).
2. B. Fisher, J. Bryant, N. Wolmark, E. Mamounas, A. Brown, E. R. Fisher, D. L. Wickerham, M. Begovic, A. DeCillis, A. Robidoux, R. G. Margolese, A. B. Cruz Jr., J. L. Hoehn, A. W. Lees, N. V. Dimitrov, and H. D. Bear, "Effect of preoperative chemotherapy on the outcome of women with operable breast cancer," *J. Clin. Oncol.* **16**(8), 2672–2685 (1998).
3. E. R. Fisher, J. Wang, J. Bryant, B. Fisher, E. Mamounas, and N. Wolmark, "Pathobiology of preoperative chemotherapy: findings from the National Surgical Adjuvant Breast and Bowel (NSABP) protocol B-18," *Cancer* **95**(4), 681–695 (2002).
4. A. Cerussi, D. Hsiang, N. Shah, M. Compton, R. Mehta, A. F. Durkin, and B. Tromberg, "Predicting response to breast cancer neoadjuvant chemotherapy using diffuse optical spectroscopy," *Proc. Natl. Acad. Sci. U.S.A.* **104**(10), 4014–4019 (2007).
5. D. B. Jakubowski, A. E. Cerussi, F. Bevilacqua, N. Shah, D. Hsiang, J. Butler, and B. J. Tromberg, "Monitoring neoadjuvant chemotherapy in breast cancer using quantitative diffuse optical spectroscopy: a case study," *J. Biomed. Opt.* **9**(1), 230–238 (2004).
6. Q. Zhu, S. H. Kurtzma, P. Hegde, S. Tannenbaum, M. Kane, M. Huang, N. G. Chen, B. Jagjivan, and K. Zarfos, "Utilizing optical tomography with ultrasound localization to image heterogeneous hemoglobin distribution in large breast cancers," *Neoplasia* **7**(3), 263–270 (2005).
7. R. Choe, A. Corlu, K. Lee, T. Durduran, S. D. Konecky, M. Grosicka-Koptyra, S. R. Arridge, B. J. Czemiecki, D. L. Fraker, A. DeMichele, B. Chance, M. A. Rosen, and A. G. Yodh, "Diffuse optical tomography of breast cancer during neoadjuvant chemotherapy: a case study with comparison to MRI," *Med. Phys.* **32**(4), 1128–1139 (2005).
8. N. Shah, J. Gibbs, D. Wolverson, A. Cerussi, N. Hylton, and B. J. Tromberg, "Combined diffuse optical spectroscopy and contrast-enhanced magnetic resonance imaging for monitoring breast cancer neoadjuvant chemotherapy: a case study," *J. Biomed. Opt.* **10**(5), 51503 (2005).
9. A. Cerussi, N. Shah, D. Hsiang, A. Durkin, J. Butler, and B. J. Tromberg, "In vivo absorption, scattering, and physiologic properties of 58 malignant breast tumors determined by broadband diffuse optical spectroscopy," *J. Biomed. Opt.* **11**(4), 044005 (2006).
10. S. S. Gorin, J. E. Heck, B. Cheng, and S. J. Smith, "Delays in breast cancer diagnosis and treatment by racial/ethnic group," *Arch. Intern. Med.* **166**(20), 2244–2252 (2006).
11. A. J. Singer and R. A. Clark, "Cutaneous wound healing," *N. Engl. J. Med.* **341**(10), 738–746 (1999).
12. M. G. Tonnesen, X. Feng, and R. A. Clark, "Angiogenesis in wound healing," *J. Investig. Dermatol. Symp. Proc.* **5**(1), 40–46 (2000).
13. F. Arnold and D. C. West, "Angiogenesis in wound healing," *Pharmacol. Ther.* **52**(3), 407–422 (1991).
14. J. K. Kiecolt-Glaser, P. T. Marucha, W. B. Malarkey, A. M. Mercado, and R. Glaser, "Slowing of wound healing by psychological stress," *Lancet* **346**(8984), 1194–1196 (1995).
15. J. E. Greenwood, B. A. Crawley, S. L. Clark, P. R. Chadwick, D. A. Ellison, B. A. Oppenheim, and C. N. McCollum, "Monitoring wound healing by odor," *J. Wound Care* **6**(5), 219–221 (1997).
16. K. Hoffmann, K. Winkler, S. el-Gammal, and P. Altmeyer, "A wound healing model with sonographic monitoring," *Clin. Exp. Dermatol.* **18**(3), 217–225 (1993).
17. T. H. Pham, O. Coquoz, J. B. Fishkin, E. Anderson, and B. J. Tromberg, "Broad bandwidth frequency domain instrument for quantitative tissue optical spectroscopy," *Rev. Sci. Instrum.* **71**(6), 2500–2513 (2000).
18. W. G. Zijlstra, A. Buursma, and W. P. Meeuwse-van der Roest, "Absorption spectra of human fetal and adult oxyhemoglobin, deoxyhemoglobin, carboxyhemoglobin, and methemoglobin," *Clin. Chem.* **37**(9), 1633–1638 (1991).
19. L. Kou, D. Labrie, and P. Chylek, "Refractive indices of water and ice in the 0.65- to 2.5- μm spectral range," *Appl. Opt.* **32**(19), 3531–3540 (1993).
20. C. Eker, "Optical characterization of tissue for medical diagnostics," PhD Thesis, Department of Physics, Lund Institute of Technology (1999).
21. J. R. Mourant, T. Fuselier, J. Boyer, T. M. Johnson, and I. J. Bigio, "Predictions and measurements of scattering and absorption over broad wavelength ranges in tissue phantoms," *Appl. Opt.* **36**(4), 949–957 (1997).
22. A. E. Cerussi, D. Jakubowski, N. Shah, F. Bevilacqua, R. Lanning, A. J. Berger, D. Hsiang, J. Butler, R. F. Holcombe, and B. J. Tromberg, "Spectroscopy enhances the information content of optical mammography," *J. Biomed. Opt.* **7**(1), 60–71 (2002).
23. D. Hom, "Wound healing in relation to scarring," *Scar Revision and Camouflage* **6**(2), 111–123 (1998).
24. K. S. Midwood, L. V. Williams, and J. E. Schwarzbauer, "Tissue repair and the dynamics of the extracellular matrix," *Int. J. Biochem. Cell Biol.* **36**(6), 1031–1037 (2004).
25. R. Cubeddu, C. D'Andrea, A. Pifferi, P. Taroni, A. Torricelli, and G. Valentini, "Effects of the menstrual cycle on the red and near-infrared optical properties of the human breast," *Photochem. Photobiol.* **72**(3), 383–391 (2000).
26. N. Shah, A. Cerussi, C. Eker, J. Espinoza, J. Butler, J. Fishkin, R. Hornung, and B. Tromberg, "Noninvasive functional optical spectroscopy of human breast tissue," *Proc. Natl. Acad. Sci. U.S.A.* **98**(8), 4420–4425 (2001).
27. B. W. Pogue, S. Jiang, H. Dehghani, C. Kogel, S. Soho, S. Srinivasan, X. Song, T. D. Tosteson, S. P. Poplack, and K. D. Paulsen, "Characterization of hemoglobin, water, and NIR scattering in breast tissue: analysis of intersubject variability and menstrual cycle changes," *J. Biomed. Opt.* **9**(3), 541–552 (2004).
28. E. White, P. Velentgas, M. T. Mandelson, C. D. Lehman, J. G. Elmore, P. Porter, Y. Yasui, and S. H. Taplin, "Variation in mammographic breast density by time in menstrual cycle among women aged 40–49 years," *J. Natl. Cancer Inst.* **90**(12), 906–910 (1998).